

Wave propagation of a functionally graded beam in thermal environments

Şeref Doğuşcan Akbaş*

*Department of Civil Engineering, Bursa Technical University,
152 Evler Mah. Eğitim Cad. 1. Damla Sok. No:2/10, Bursa, 16330, Turkey*

(Received October 20, 2014, Revised February 07, 2015, Accepted June 16, 2015)

Abstract. In this paper, the effect of material-temperature dependent on the wave propagation of a cantilever beam composed of functionally graded material (FGM) under the effect of an impact force is investigated. The beam is excited by a transverse triangular force impulse modulated by a harmonic motion. Material properties of the beam are temperature-dependent and change in the thickness direction. The Kelvin–Voigt model for the material of the beam is used. The considered problem is investigated within the Euler-Bernoulli beam theory by using energy based finite element method. The system of equations of motion is derived by using Lagrange's equations. The obtained system of linear differential equations is reduced to a linear algebraic equation system and solved in the time domain and frequency domain by using Newmark average acceleration method. In order to establish the accuracy of the present formulation and results, the comparison study is performed with the published results available in the literature. Good agreement is observed. In the study, the effects of material distributions and temperature rising on the wave propagation of the FGM beam are investigated in detail.

Keywords: wave propagation; temperature dependent physical properties; functionally graded materials; beam

1. Introduction

Elastic wave propagation through the monitored part is of considerable interest in many fields. The most striking example of the engineering applications is detection of damage or/and material difference in the investigated media. By investigating the character of waves, the type and position of damage can be determined.

Functionally graded materials (FGMs) are a new generation of composites where the volume fraction of the FGM constituents vary gradually, giving a non-uniform microstructure with continuously graded macro properties such as elasticity modulus, density, heat conductivity, etc. Typically, in a FGM, one face of a structural component is ceramic that can resist severe thermal loading and the other face is metal which has excellent structural strength. FGMs consisting of heat-resisting ceramic and fracture-resisting metal can improve the properties of thermal barrier systems because cracking and delamination, which are often observed in conventional layered

*Corresponding author, Professor, Ph.D., E-mail: serefda@yahoo.com

composites, are reduced by proper smooth transition of material properties. Since the concept of FGMs has been introduced in 1980s, these new kinds of materials have been employed in many engineering application fields, such as aircrafts, space vehicles, defense industries, electronics and biomedical sectors, to eliminate stress concentrations, to relax residual stresses, and to enhance bonding strength. Because of the wide material variations and applications of FGMs, it is important to study the responses of FGM structures to mechanical and other loadings. With the increased use of FGMs, understanding the mechanical behavior and safe performance of cracked FGM structures is very important.

In the last decades, much more attention has been given to the elastic wave propagation of beam structures. Teh and Huang (1981) studied an analytical model, based on the elasticity equations, to investigate wave propagation in generally orthotropic beams. A finite element technique is developed for studying the flexural wave propagation in elastic Timoshenko and Bernoulli-Euler beams by Yokoyama and Kishida (1982). Wave propagation in a split beam is analyzed by treating each section separately as a waveguide and imposing appropriate connectivities at their joints by Farris and Doyle (1989). A direct mathematical approach method is developed to study the problem of coupled longitudinal and flexural wave propagation in a periodically supported infinite long beam by Lee and Yeen (1990). A spectral super-element model was used in Gopalakrishnan and Doyle (1995) to model transverse crack in isotropic beam and the dynamic stress intensity factor was obtained accurately under impact type loading. Palacz and Krawczuk (2002) investigated longitudinal wave propagation in a cracked rod by using the spectral element method. The use of the wave propagation approach combined with a genetic algorithm and the gradient technique for damage detection in beam-like structure is investigated by Krawczuk (2002). Krawczuk *et al.* (2002) studied a new finite spectral element of a cracked Timoshenko beam for modal and elastic wave propagation analysis. Usuki and Maki (2003) formulated an equation of motion for a beam according to higher-order beam theory using Reissner's principle. They derived the Laplace transform of the equation and investigated wave-propagation behavior under transverse impact. A method of crack detection in beam is provided by wavelet analysis of transient flexural wave by Tian *et al.* (2003). Kang *et al.* (2003) applied the wave approach based on the reflection, transmission and propagation of waves to obtain the natural frequencies of finite curved beams. A spectral finite element with embedded transverse crack is developed and implemented to simulate the diagnostic wave scattering in composite beams with various forms of transverse crack by Kumar *et al.* (2004). The wave propagation model investigated herein is based on the known fact that material discontinuities affect the propagation of elastic waves in solids by Ostachowicz *et al.* (2004). A spectral finite element model for analysis of flexural-shear coupled wave propagation in laminated and delaminated, multilayer composite beams is presented by Palacz *et al.* (2005a, b). A new spectral element is formulated to analyse wave propagation in an anisotropic inhomogeneous beam by Chakraborty and Gopalakrishnan (2005). Watanabe and Sugimoto (2005) studied flexural wave propagation in a spatially periodic structure consisting of identical beams of finite length. Vinod *et al.* (2007) investigated a formulation of an approximate spectral element for uniform and tapered rotating Euler-Bernoulli beams. An experimental method of detecting damage using the flexural wave propagation characteristics is proposed by Park (2008). Chouvion *et al.* (2010) studied a systematic wave propagation approach for the free vibration analysis of networks consisting of slender, straight and curved beam elements and complete rings. Frikha *et al.* (2011) investigated physical analysis of the effect of axial load on the propagation of elastic waves in helical beams. Kocatürk *et al.* (2011) studied wave propagation of a piecewise homogenous cantilever beam

under impact force. Kocatürk and Akbas (2013) investigated wave propagation of a microbeam with the modified couple stress theory. In a recent study, wave propagation and localization in periodic and randomly disordered periodic piezoelectric axial-bending coupled beams are studied by Zhu *et al.* (2013). Akbaş (2014a) investigated the effect of the elastic foundation on the wave propagation of the cracked beams. Also, Akbaş (2014b) studied the estimation of the crack locations and the effect of cracks on the wave propagation of the circular beams. Islam *et al.* (2014) studied the torsional wave propagation and vibration of nanostructures based on nonlocal elasticity theory. Akbaş (2015) investigated the effect of the cracks on the wave propagation of the FG beam.

In recent years, the wave propagation behavior of FG structures has been a topic of active research. Chakraborty and Gopalakrishnan (2004) studied wave propagation in anisotropic inhomogeneous layered media due to high frequency impact loading by using a new spectral layer element. Li *et al.* (2004) investigated the Love waves in a layered functionally graded piezoelectric structure. Chakraborty *et al.* (2005) used the thin-layer method to study the propagation of waves in inhomogeneous piezocomposite layered media caused by mechanical loading and electrical excitation. Sridhar *et al.* (2007) developed an effective pseudo-spectral finite element method for wave propagation analysis in anisotropic and inhomogeneous structures with or without vertical and horizontal cracks. Dineva *et al.* (2007) studied the elastic wave propagation in cracked, functionally graded materials with elastic parameters. Du *et al.* (2007) investigated the Love waves in functionally graded piezoelectric material layer bonded to a semi-infinite homogeneous solid with an exact approach. Bin *et al.* (2008) solved the propagation of harmonic waves in functionally graded magneto-electro-elastic plates composed of piezoelectric materials. Aksoy and Şenocak (2009) analyzed the wave propagation in FG and layered materials by using space-time discontinuous Galerkin method. Jiangong and Qiujuan (2010) investigated wave characteristics in magneto-electro-elastic FG spherical curved plates based on the Legendre orthogonal polynomial series expansion approach. Nonlinear thermoelasticity, vibration, and stress wave propagation analyses of thick-walled FG cylinders with temperature-dependent properties are examined by Shariyat *et al.* (2010). Sun and Luo (2011a, b, c, d and 2012) analyzed the wave propagation and transient response of an infinite FG plates under a point impact load. Safari-Kahnaki *et al.* (2011) investigated transient stress field and thermo-elastic stress wave propagation of FG thick hollow cylinder under arbitrary thermomechanical shock loading. Cao *et al.* (2012) studied the propagation behaviour of Lamb waves of th FG piezoelectric-piezomagnetic material plate with material parameters. Liu and Lu (2012) examined the dynamic stability of an Euler–Bernoulli beams resting on the elastic foundation including the stress wave effect. Boudarba *et al.* (2013) studied the thermomechanical bending response of functionally graded plates resting on Winkler-Pasternak elastic foundations. Tounsi *et al.* (2013) investigated thermoelastic bending analysis of functionally graded sandwich plates with A refined trigonometric shear deformation theory taking into account transverse shear deformation effects. Zidi *et al.* (2014) studied bending response of functionally graded plates resting on elastic foundation and subjected to hygro-thermo-mechanical loading. Molaei Najafabadi *et al.* (2014) investigated the effect of thermal wave propagation on thermoelastic behavior of FG materials in a slab symmetrically surface heated using analytical modeling. Bourada *et al.* (2015) investigated developed a simple and refined trigonometric higher-order beam theory for bending and vibration of functionally graded beams. Mahi *et al.* (2015) investigated A new hyperbolic shear deformation theory applicable to bending and free vibration analysis of isotropic, functionally graded, sandwich and laminated composite plates. Ait Yahia *et al.* (2015) studied wave propagation in functionally

graded plates with different higher-order shear deformation plate theories.

It is seen from literature that the effect of the temperature rising on the wave propagation of FG beams has not been broadly investigated. It is known that with investigation elastic wave propagation of the structures, it can be detected the mechanical changes of the structures. Hence, with using wave propagation techniques, it can be investigated and detected the mechanical changes FG structures for temperature rising by investigating the character of waves. A better understanding of the mechanism of how the different material distributions and temperature change response of wave propagation of a FGM beam is necessary, and is a prerequisite for further exploration and application of the FGM beams. Hence, the effects of different material distributions and temperature rising on wave propagation of FG beams are investigated in detail.

In this study, the effect of material-temperature dependent on the wave propagation in a cantilever FG beam under the effect of an impact force is studied. The considered problem is investigated within the Euler-Bernoulli beam theory by using energy based finite element method. The Kelvin–Voigt model for the material of the beam is used. The material properties of the beam are temperature-dependent and change in the thickness direction of the beam. Three homogenization methods are deployable for the computation of the material properties namely: (1) the power law distribution; (2) the exponential distribution; and (3) the Mori–Tanaka scheme. The temperature is assumed to be uniform and only varies in the thickness of the beam. The system of equations of motion is derived by using Lagrange’s equations. The obtained system of linear differential equations is reduced to a linear algebraic equation system and solved in the time domain and frequency domain by using Newmark average acceleration method. In order to establish the accuracy of the present formulation and results, the comparison study is performed with the published results available in the literature. Good agreement is observed. In the study, the effects of material distributions and temperature rising on the wave propagation of the FG beam are investigated in detail.

2. Theory and formulations

Consider a cantilever FGM beam of length L , width b , thickness h , as shown in Fig. 1. The beam is subjected to an impact force in the transverse direction as seen from Fig. 1.

In this study, the material properties are both temperature-dependent and position-dependent. The effective material properties of the functionally graded beam, P , i.e., Young’s modulus E , and

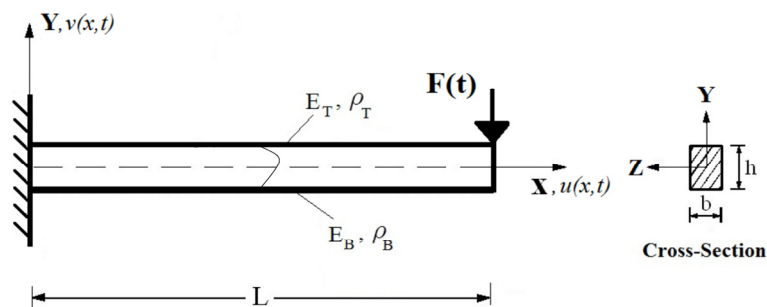


Fig. 1 A cantilever FG beam subjected to an impact force and cross-section

mass density ρ vary continuously in the height direction (Y axis) and a function of temperature T (see Touloukian (1967)) as follows

$$P(T) = P_0(P_{-1}T^{-1} + 1 + P_1T + P_2T^2 + P_3T^3) \quad (1)$$

where P_T and P_B are the material properties of the top and the bottom surfaces of the beam that depends on temperature (T), $T = T_0 + \Delta T$, where T_0 is installation temperature and ΔT is the uniform temperature rise.

Material properties of the FG beam are temperature-dependent and change in the thickness direction. Three homogenization methods are deployable for the computation of the material properties $P(Y)$ namely: (1) the power law distribution; (2) the exponential distribution; and (3) the Mori–Tanaka scheme. For the power law distribution, the material properties are as follows

$$P(Y, T) = (P_T(T) - P_B(T)) \left(\frac{Y}{h} + \frac{1}{2} \right)^n + P_B(T) \quad (2)$$

It is clear from Eq. (3) that when $X = -h/2$, $P = P_B$, and when $X = h/2$, $P = P_T$. Where n is the non-negative power-law exponent which dictates the material variation profile through the height direction of the beam. In Eq. (1), P_{-1} , P_0 , P_1 , P_2 and P_3 indicate the coefficients of temperature T and are unique to the constituent materials. In this study, the unit of the temperature is Kelvin (K), the unit of the Young's modulus E is Pascal (Pa) and the unit of the mass density ρ is kg/m^3 .

For the exponential distribution, the material properties are as follows

$$P(Y, T) = P_0(Y, T)e^{bY} \quad (3)$$

where P_0 is the material properties at the midplane ($Y = 0$) of the beam. b is a constant characterizing the gradual variation of the material properties along thickness direction. When $b = 0$, the material of the beam is homogeneous. According to Eq. (14) that when $Y = -h/2$, $P = P_B$ (P_B is material properties of the bottom). When $Y = h/2$, $P = P_T$ and $r = r_T$ (E_T and r_T is the material properties of the top). In this study, the ratio of material properties indicates as P_R which ratio of material properties of bottom and top surfaces of the beam (P_B / P_T). When $P_R = 1$, the material of the beam is homogeneous. In other words, when $P_R = 1$, $b = 0$ according to Eq. (3).

For Mori–Tanaka scheme, the material properties is given as (Shen and Wang 2012)

$$P(Y, T) = P_B(T) + (P_T(T) - P_B(T)) \left(\frac{V_T}{1 + (1 - V_T)(P_T/P_B - 1)(1 + n)/(3 - 3n)} \right) \quad (4)$$

Where $V_T = (0.5 + y/h)^n$ is the volume fraction of the top materials.

The beams considered in numerical examples are made of Zirconia and Aluminum Oxide. The bottom surface of the functionally graded beam is Zirconia and the top surface of the functionally graded beam is Aluminum Oxide. The coefficients of temperature T for Zirconia and Aluminum Oxide are listed in Table 1 and 2 (from Reddy and Chin 1998).

According to the coordinate system (X, Y, Z) shown in Fig. 1, based on Euler-Bernoulli beam theory, the axial and the transverse displacement field are expressed as

$$u(X, Y, t) = u_0(X, t) - Y \frac{\partial v_0(X, t)}{\partial X} \quad (5)$$

Table 1 The coefficients of temperature T for Zirconia (from Reddy and Chin 1998)

The material properties	P_0	P_{-1}	P_1	P_2	P_3
Thermal expansion coefficient α_X (1/K)	12.766×10^{-6}	0	-1.491×10^{-3}	1.0006×10^{-5}	-6.778×10^{-11}
Young's modulus E (Pa)	244.27×10^9	0	-1.371×10^{-3}	1.214×10^{-6}	-3.681×10^{-10}
Poisson's ratio n	0.2887	0	1.133×10^{-4}	0	0
Mass density r (kg/m ³)	5700	0	0	0	0

Table 2 The coefficients of temperature T for Aluminum Oxide (from Reddy and Chin 1998)

The material properties	P_0	P_{-1}	P_1	P_2	P_3
Thermal expansion coefficient α_X (1/K)	6.8269×10^{-6}	0	1.838×10^{-4}	0	0
Young's modulus E (Pa)	349.55×10^9	0	-3.853×10^{-4}	4.027×10^{-7}	-1.673×10^{-10}
Poisson's ratio n	0.26	0	0	0	0
Mass density r (kg/m ³)	2700	0	0	0	0

$$v(X, Y, t) = v_0(X, t) \quad (6)$$

Where u_0 and v_0 are the axial and the transverse displacements in the mid-plane, t indicates time. Using Eqs. (5) and (6), the linear strain- displacement relation can be obtained

$$\varepsilon_{xx} = \frac{\partial u}{\partial X} = \frac{\partial u_0(X, t)}{\partial X} - Y \frac{\partial^2 v_0(X, t)}{\partial X^2} \quad (7)$$

According to Hooke's law, constitutive equations of the FGM beam are as follows

$$\begin{aligned} \sigma_{xx} &= E(Y, T) \varepsilon = E(Y, T) [\varepsilon_{xx} - \alpha(Y, T) \Delta T] \\ &= E(Y, T) \left[\frac{\partial u_0(X, t)}{\partial X} - Y \frac{\partial^2 v_0(X, t)}{\partial X^2} - \alpha(Y, T) \Delta T \right] \end{aligned} \quad (8)$$

Where σ_{xx} and ε are normal stresses and normal strains in the X direction, respectively. Based on Euler-Bernoulli beam theory, the elastic strain energy (U_i) of the beam is expressed as

$$U_i = \frac{1}{2} \int_0^L \int_A \sigma_{xx} \varepsilon dA dX \quad (9)$$

By substituting Eqs. (7) and (8) into Eq. (9), elastic strain energy (U_i) can be rewritten as follows

$$\begin{aligned} U_i &= \frac{1}{2} \int_0^L \left[A_{xx} \left(\frac{\partial u_0}{\partial x} \right)^2 - 2 B_{xx} \left(\frac{\partial u_0}{\partial x} \right) \left(\frac{\partial^2 v_0}{\partial x^2} \right) + D_{xx} \left(\frac{\partial^2 v_0}{\partial x^2} \right)^2 - A_{xt} \left(\frac{\partial u_0}{\partial x} \right) \right. \\ &\quad \left. + 2 A_{yt} \left(\frac{\partial^2 v_0}{\partial x^2} \right) + A_{xt} \alpha(Y, T) \Delta T \right] dX \end{aligned} \quad (10)$$

where

$$(A_{XX}, B_{XX}, D_{XX}) = \int_A E(Y, T)(1, Y, Y^2) dA \quad (11a)$$

$$(A_{XT}, A_{YT}) = \int_A E(Y, T) \alpha(Y, T) \Delta T (1, Y) dA \quad (11b)$$

Kinetic energy (V) of the FGM beam are expressed as follows

$$V = \frac{1}{2} \int_0^L \int_A \rho(Y, T) \left[\left(\frac{\partial u}{\partial t} \right)^2 + \left(\frac{\partial v}{\partial t} \right)^2 \right] dA dX \quad (12)$$

By substituting Eqs. (5) and (6) into Eq. (12), Kinetic energy (V) can be rewritten as follows

$$V = \frac{1}{2} \int_0^L \left[I_1 \left(\frac{\partial u_0}{\partial t} \right)^2 - 2I_2 \left(\frac{\partial u_0}{\partial t} \right) \left(\frac{\partial^2 v_0}{\partial X \partial t} \right)^2 + I_1 \left(\frac{\partial v_0}{\partial t} \right)^2 + I_3 \left(\frac{\partial^2 v_0}{\partial X \partial t} \right)^2 \right] dX \quad (13)$$

where

$$(I_1, I_2, I_3) = \int_A \rho(Y, T)(1, Y, Y^2) dA \quad (14)$$

The potential energy of the external load can be written as

$$U_e = - \int_{x=0}^L F(X, t) v(X, t) dx \quad (15)$$

The Kelvin–Voigt model for the FGM beam is used. The constitutive relations for the Kelvin–Voigt model between the stresses and strains become

$$\sigma = E(Y, T) \left(\varepsilon + \eta(Y, T) \frac{\partial \varepsilon}{\partial t} \right) \quad (16)$$

where η is the damping ratios, as follows

$$\eta(Y, T) = \frac{c(Y)}{E(Y, T)} \quad (17)$$

where c is the coefficient of damping of the beam. the dissipation function of the beam is expressed as

$$R = \frac{1}{2} \int_V E(Y, T) \left(\eta(Y, T) \frac{\partial \varepsilon_{XX}}{\partial t} \right)^2 dV \quad (18)$$

By substituting Eq. (7) into Eq. (18) and reducing the volume integral to a one-dimensional integral, the dissipation function (R) can be rewritten as follows

$$R = \frac{1}{2} \int_0^L \left[C_1 \left(\frac{\partial}{\partial X} \left(\frac{\partial u_0}{\partial t} \right) \right)^2 - 2C_2 \left(\frac{\partial}{\partial X} \left(\frac{\partial u_0}{\partial t} \right) \right) \left(\frac{\partial^2}{\partial X^2} \left(\frac{\partial v_0}{\partial t} \right) \right) + C_3 \left(\frac{\partial^2}{\partial X^2} \left(\frac{\partial v_0}{\partial t} \right) \right)^2 \right] dX \quad (19)$$

where

$$(C_1, C_2, C_3) = \int_A E(Y, T) \eta(Y, T) (1, Y, Y^2) dA \quad (20)$$

Lagrangian functional of the problem is given as follows

$$I = T - (U_i + U_e) \quad (21)$$

The problem is solved by using Lagrange’s equations and time integration method of Newmark (1959).

Total nodal displacements q which is written for a two-node beam element, each node has three degrees of freedom, shown in Fig. 2 are defined as follows

$$\{q(t)\}_{(e)} = [u_i^{(e)}(t), v_i^{(e)}(t), \theta_i^{(e)}(t), u_j^{(e)}(t), v_j^{(e)}(t), \theta_j^{(e)}(t)]^T \quad (22)$$

The displacement field of the finite element is expressed in terms of nodal displacements as follows

$$\begin{aligned} u^{(e)}(X, t) &= \varphi_1^{(U)}(X) u_i(t) + \varphi_2^{(U)}(X) u_j(t) \\ &= [\varphi^{(U)}] \begin{Bmatrix} u_i \\ u_j \end{Bmatrix} = [\varphi^{(U)}] \{q\}_U \end{aligned} \quad (23)$$

$$\begin{aligned} v^{(e)}(X, t) &= \varphi_1^{(V)}(X) v_i(t) + \varphi_2^{(V)}(X) \theta_i(t) + \varphi_3^{(V)}(X) v_j(t) + \varphi_4^{(V)}(X) \theta_j(t) \\ &= [\varphi^{(V)}] \begin{Bmatrix} v_i \\ \theta_i \\ v_j \\ \theta_j \end{Bmatrix} = [\varphi^{(V)}] \{q\}_V \end{aligned} \quad (24)$$

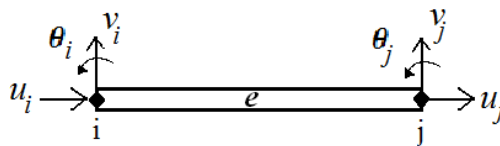


Fig. 2 A two-node beam element

where u_i, v_i and q_i are axial displacements, transverse displacements and slopes at the two end nodes of the beam element, respectively. $j_i^{(U)}$ and $j_i^{(V)}$ are Hermitian shape functions for axial and transverse degrees of freedom, respectively, which are given in Appendix.

By substituting Eqs. (23) and (24) into Eqs. (10), (11) and (19), energy functions can be rewritten as follows

$$\begin{aligned}
U_i = \frac{1}{2} \int_0^L & [A_{xx} \left(\left[\frac{\partial \varphi^{(U)}}{\partial X} \right] \{q\}_U \right)^2 - 2B_{xx} \left(\left[\frac{\partial \varphi^{(U)}}{\partial X} \right] \{q\}_U \right) \left(\left[\frac{\partial^2 \varphi^{(V)}}{\partial X^2} \right] \{q\}_V \right) \\
& + D_{xx} \left(\left[\frac{\partial^2 \varphi^{(V)}}{\partial X^2} \right] \{q\}_V \right)^2 - A_{xT} \left(\left[\frac{\partial \varphi^{(U)}}{\partial X} \right] \{q\}_U \right) \\
& + 2A_{yT} \left(\left[\frac{\partial^2 \varphi^{(V)}}{\partial X^2} \right] \{q\}_V \right) + A_{xT} \alpha(Y, T) \Delta T] dX
\end{aligned} \quad (25)$$

$$\begin{aligned}
T = \frac{1}{2} \int_0^L & [I_1 \left(\left[\frac{\partial \varphi^{(U)}}{\partial t} \right] \{q\}_U \right)^2 - 2I_2 \left(\left[\frac{\partial \varphi^{(U)}}{\partial t} \right] \{q\}_U \right) \left(\left[\frac{\partial^2 \varphi^{(V)}}{\partial X \partial t} \right] \{q\}_V \right)^2 \\
& + I_1 \left(\left[\frac{\partial \varphi^{(V)}}{\partial t} \right] \{q\}_V \right)^2 + I_3 \left(\left[\frac{\partial^2 \varphi^{(V)}}{\partial X \partial t} \right] \{q\}_V \right)^2] dX
\end{aligned} \quad (26)$$

$$\begin{aligned}
R = \frac{1}{2} \int_0^L & [C_1 \left(\frac{\partial}{\partial X} \left(\left[\frac{\partial \varphi^{(U)}}{\partial t} \right] \{q\}_U \right) \right)^2 - 2C_2 \left(\frac{\partial}{\partial X} \left(\left[\frac{\partial \varphi^{(U)}}{\partial t} \right] \{q\}_U \right) \right) \\
& \left(\frac{\partial^2}{\partial X^2} \left(\left[\frac{\partial \varphi^{(V)}}{\partial t} \right] \{q\}_V \right) \right) + C_3 \left(\frac{\partial^2}{\partial X^2} \left(\left[\frac{\partial \varphi^{(V)}}{\partial t} \right] \{q\}_V \right) \right)^2] dX
\end{aligned} \quad (27)$$

After substituting Eqs. (23) and (24) into Eq. (21) and then using the Lagrange's equations gives the following equation

$$\frac{\partial I}{\partial q_k^{(e)}} - \frac{d}{dt} \frac{\partial I}{\partial \dot{q}_k^{(e)}} + Q_{D_k} = 0, \quad k = 1, 2, 3, 4, 5, 6 \quad (28)$$

where

$$Q_{D_k} = - \frac{\partial R}{\partial \dot{q}_k^{(e)}}, \quad (29)$$

Q_{D_k} is the generalized damping load which can be obtained from the dissipation function by differentiating R with respect to $\dot{q}_k^{(e)}$. Where $\dot{q}_k^{(e)}$ indicates the time derivatives of nodal displacements q .

The Lagrange's equations yield the system of equations of motion for the finite element and by use of usual assemblage procedure the following system of equations of motion for the whole system can be obtained as follows

$$[K] \{q(t)\} + [D] \{\dot{q}(t)\} + [M] \{\ddot{q}(t)\} = \{F(t)\} \quad (30)$$

where, $[K]$ is the stiffness matrix, $[D]$ is the damping matrix, $[M]$ is mass matrix and $\{F(t)\}$ is the load vector.

The components of the stiffness matrix $[K]$

$$[K] = \begin{bmatrix} [K^A] & [K^B] \\ [K^B]^T & [K^D] \end{bmatrix}, \quad (31a)$$

where

$$[K^A] = \int_0^{L_e} A_{XX} \left[\frac{d\varphi^{(u)}}{dX} \right]^T \left[\frac{d\varphi^{(u)}}{dX} \right] dX, \quad (31b)$$

$$[K^B] = - \int_0^{L_e} B_{XX} \left[\frac{d^2\varphi^{(v)}}{dX^2} \right]^T \left[\frac{d\varphi^{(u)}}{dX} \right] dX, \quad (31c)$$

$$[K^D] = \int_0^{L_e} D_{XX} \left[\frac{d^2\varphi^{(v)}}{dX^2} \right]^T \left[\frac{d^2\varphi^{(v)}}{dX^2} \right] dX, \quad (31d)$$

Where L_e indicates the length of the finite beam element. The mass matrix $[M]$ can be expressed as a sum of four sub-matrices as shown below

$$[M] = [M_U] + [M_V] + [M_\theta] + [M_{U\theta}] \quad (32)$$

Where $[M_U]$, $[M_V]$ and $[M_\theta]$ are the contribution of u , v and q degree of freedom to the mass matrix, $[M_{Uq}]$ is coupling mass matrix due to coupling between u and q . Explicit forms of $[M]$ are given as follows

$$[M_U] = \int_0^{L_e} I_1 [\varphi^{(u)}]^T [\varphi^{(u)}] dX, \quad (33a)$$

$$[M_V] = \int_0^{L_e} I_1 [\varphi^{(v)}]^T [\varphi^{(v)}] dX, \quad (33b)$$

$$[M_\theta] = \int_0^{L_e} I_1 \left[\frac{d\varphi^{(v)}}{dX} \right]^T \left[\frac{d\varphi^{(v)}}{dX} \right] dX, \quad (33c)$$

$$[M_{U\theta}] = - \int_0^{L_e} I_2 \left([\varphi^{(u)}]^T \left[\frac{d\varphi^{(v)}}{dX} \right] + \left[\frac{d\varphi^{(v)}}{dX} \right]^T [\varphi^{(u)}] \right) dX, \quad (33d)$$

The components of the damping matrix $[D]$

$$[D] = \begin{bmatrix} [D^A] & [D^B] \\ [D^B]^T & [D^D] \end{bmatrix}, \quad (34a)$$

where

$$[D^A] = \int_0^{L_e} C_1 \left[\frac{d\varphi^{(u)}}{dX} \right]^T \left[\frac{d\varphi^{(u)}}{dX} \right] dX, \quad (34b)$$

$$[D^B] = - \int_0^{L_c} C_2 \left[\frac{d^2 \varphi^{(v)}}{dX^2} \right]^T \left[\frac{d\varphi^{(v)}}{dX} \right] dX, \quad (34c)$$

$$[D^D] = \int_0^{L_c} C_3 \left[\frac{d^2 \varphi^{(v)}}{dX^2} \right]^T \left[\frac{d^2 \varphi^{(v)}}{dX^2} \right] dX, \quad (34d)$$

The load vector $\{F(t)\}$ is expressed as

$$\{F(t)\} = \int_{x=0}^{L_c} \{\varphi(X)\}^T F(X,t) dX \quad (35)$$

The motion equations which is given by Eq. (30), are solved in the time domain by using Newmark average acceleration method (Newmark 1959).

3. Numerical results

In the numerical examples, the effects of the different material distributions and temperature rising on the wave propagations of the FG beam are presented in figures. The beams considered in numerical examples are made of Zirconia and Aluminum Oxide. The bottom surface of the FG beam is Zirconia and the top surface of the FG beam is Aluminum Oxide. When the power index $n = 0$, the beam material is reduced to full Aluminum Oxide (homogeneous Aluminum Oxide). The coefficients of temperature T for Zirconia and Aluminum Oxide are listed in Tables 1 and 2 (from Reddy and Chin 1998). In this study, the unit of the temperature is Kelvin (K). In numerical examples, the initial temperature (installation temperature) of the beam is assumed to be $T_0 = 300$ K. In numerical calculations, the number of finite elements is taken as 100 elements. Unless otherwise stated, it is assumed that the width of the beam is $b = 0.1$ m, height of the beam is $h = 0.1$ m and length of the beam is $L = 3$ m in the numerical results. In the numerical integrations, five-point Gauss integration rule is used.

Numerical calculations in the time domain are made by using Newmark average acceleration method. The system of linear differential equations which are given by Eq. (30), is reduced to a linear algebraic system of equations by using average acceleration method. The beam is excited by a transverse triangular force impulse (with a peak value 1 N) modulated by a harmonic function (Fig. 3) (Ostachowicz *et al.* 2004). In this study, higher frequency excitation impulse is used for detection of the cracks. The frequencies used in this technique are much higher than those typically used in modal analysis based methods but are lower than the frequencies used for ultrasonic testing. In our case the excited frequencies lies in the range between 200 and 1200 kHz, with dominant one about 700 kHz. At such high frequencies, the response is dominated by the local mode and the wavelength of the excitation is small enough to detect incipient or potentially significant damage.

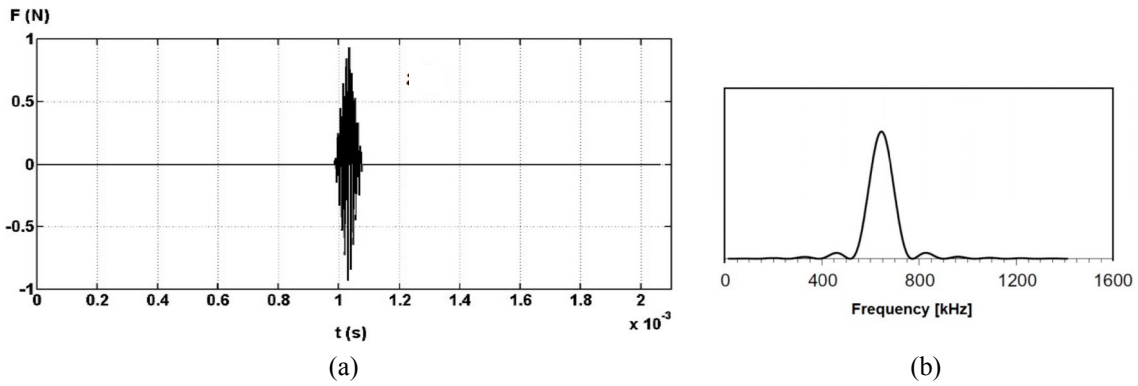


Fig. 3 The shape of the excitation impulse in the (a) time domain; and (b) frequency domain

Table 3 Comparison of the dimensionless fundamental frequency $\bar{\omega}_i$ of intact FG beams

P_R	Present	Yang and Chen (2008)	Ke <i>et al.</i> (2009)
0.2	0.8283	0.83	0.8235
1	0.8786	0.88	0.8752
5	0.8283	0.83	0.8235

In order to establish the accuracy of the present formulation and the computer program developed by the author, the results obtained from the present study are compared with the available results in the literature. For this purpose, the dimensionless fundamental frequency

$$\left(\bar{\omega} = \frac{\omega}{\sqrt{D_{xx}/I_1}} \right)$$

of a FG cantilever beam according to the exponential distribution are calculated for different exponential ratios P_R for $L/h = 20$ compared with those of Yang and Chen (2008) and Ke *et al.* (2009). As seen from Table 3, the present results are in good agreement with that the results of Yang and Chen (2008) and Ke *et al.* (2009).

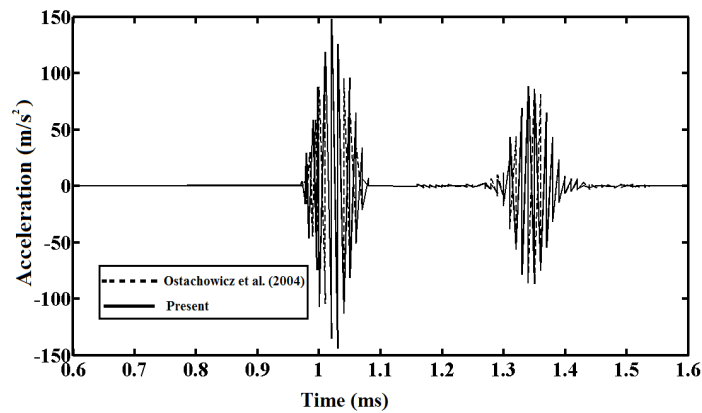


Fig. 4 Transverse accelerations at the free end of the homogeneous beam

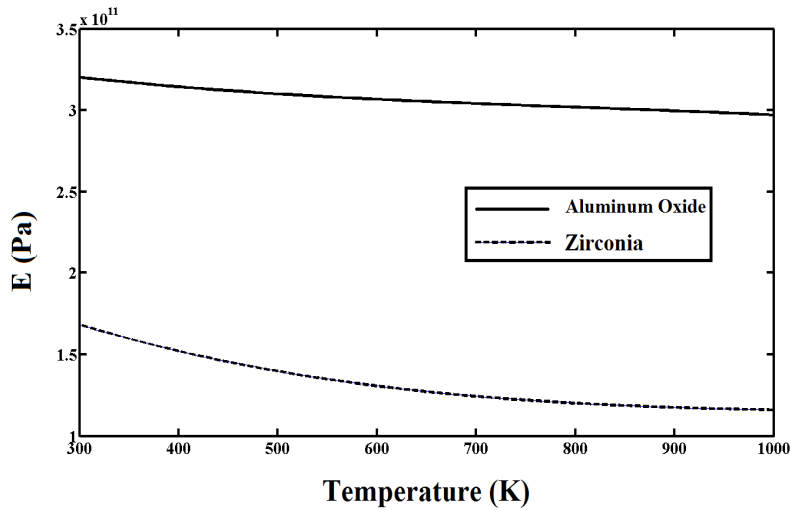


Fig. 5 Young’s Modulus versus temperature rising for Zirconia and Aluminum Oxide

To further verify the present results, the transverse accelerations at the free end of the homogeneous cantilever beam are plotted for compared with those of Ostachowicz *et al.* (2004) for $b = 0.02$ m, $h = 0.02$ m, $E = 72.7$ GPa, Poisson ratio = 0.33 and mass density $\rho = 2700$ kg/m³. It is clearly seen that the curves of Fig. 4 of the present study are very close to those of Fig. 4 of Li *et al.* Ostachowicz *et al.* (2004).

Young’s Modulus versus temperature rising is illustrated in Fig. 5 by using Eqs. (1) and (2) for Zirconia and Aluminum Oxide.

It is seen from Fig. 5 that with increase in temperature, Young’s modulus decreases. Because, with the temperature increase, the intermolecular distances of the material increase and inter-

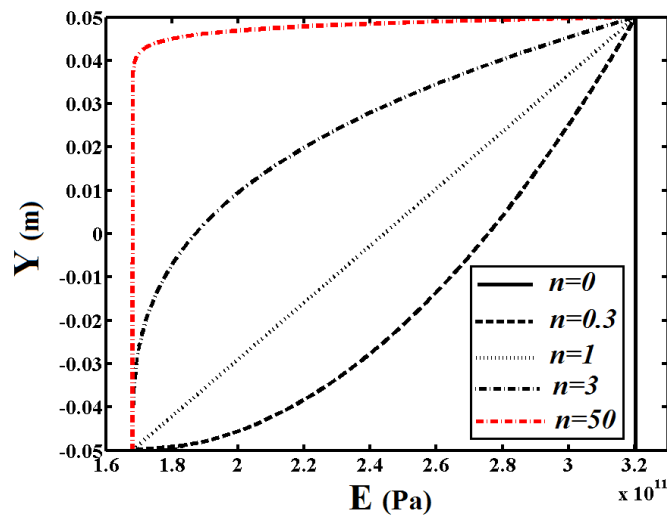


Fig. 6 Young’s Modulus distributions along the height of the beam for some given values of the power-law exponent n for the temperature environment $T = 400$ K

molecular forces decrease. As a result, the strength of the material decreases.

In Fig. 6, the variations of material properties (Young's Modulus) distributions along the height of the beam are presented for some given values of the power-law exponent n for the temperature environment $T = 400$ K.

It is seen from Fig. 6 that, when the material power law index n increases, Young's modulus decreases. Because when the material power law index n increase, the material of the beam get close to the bottom material (pure Zirconia) and it is known from the physical properties of the pure Zirconia and the top material (Aluminum Oxide) that the Young modulus of pure Aluminum Oxide is approximately greater than that of Zirconia.

In Fig. 7, the variations of Young's Modulus distributions along the height of the beam are presented for some given values of the temperature T and some given values of the power-law exponent with temperature dependent physical properties.

It is seen from Fig. 7 that with increase in temperature, the Young's Modulus of beam varies considerably. Also, it is seen from Fig. 7 that, the material power law index n play an important role on the properties of the materials.

In Figs. 8-15, the effects of the uniform temperature rising on the wave propagation of the FG beam are investigated for the power law distribution. For this purpose, the effect of the temperature on the transverse accelerations at the free end of the FG cantilever beam are illustrated in Figs. 8, 9, 10 and 11 for the $n = 0$, $n = 0.5$, $n = 1$ and $n = 2$, respectively. Also, the effect of the temperature on the transverse displacements at the free end of the FG cantilever beam on the frequency domain are illustrated in Figs. 12, 13, 14 and 15 for the $n = 0$, $n = 0.3$, $n = 1$ and $n = 3$, respectively.

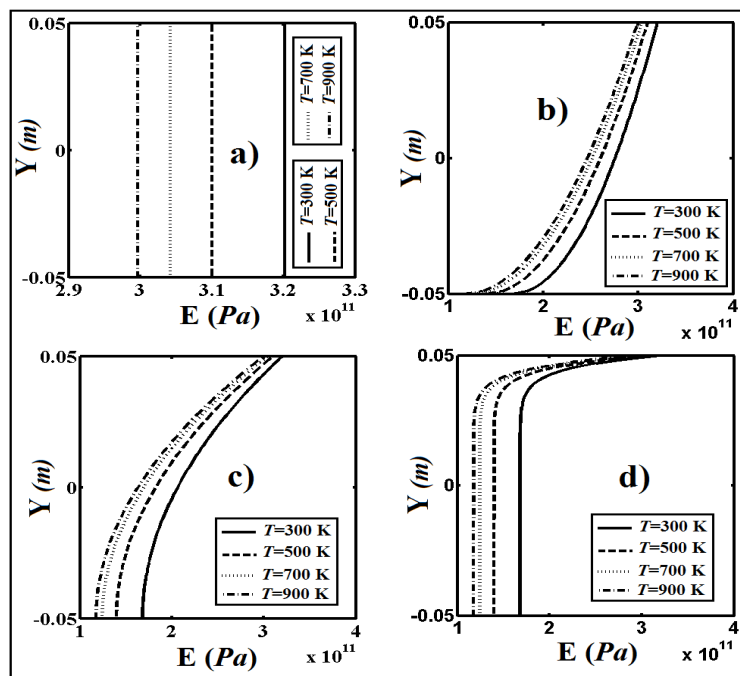


Fig. 7 Variations of Young's Modulus with some given values of the temperature T : (a) $n = 0$; (b) $n = 0.5$; (c) $n = 2$; and (d) $n = 20$

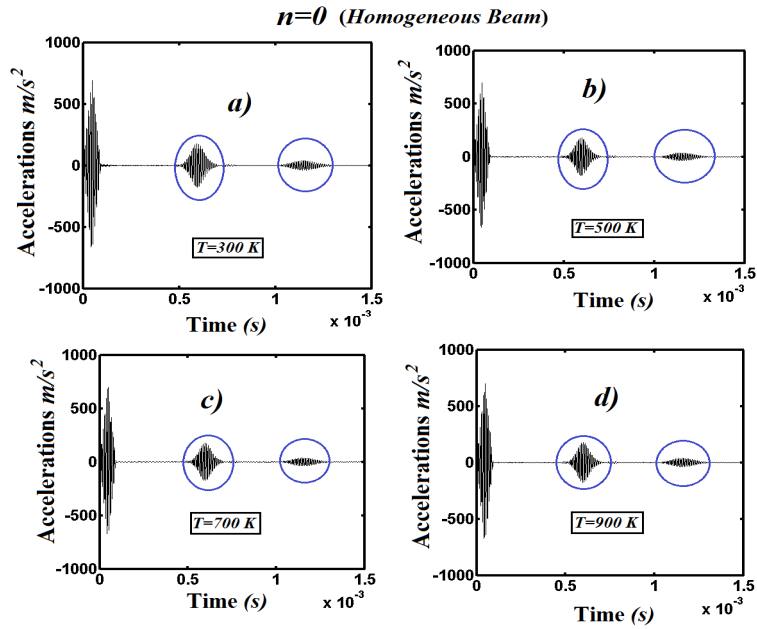


Fig. 8 Transverse accelerations at the free end of the FG beam for $n = 0$. (a) $T = 300\text{ K}$; (b) $T = 500\text{ K}$; (c) $T = 700\text{ K}$; and (d) $T = 900\text{ K}$

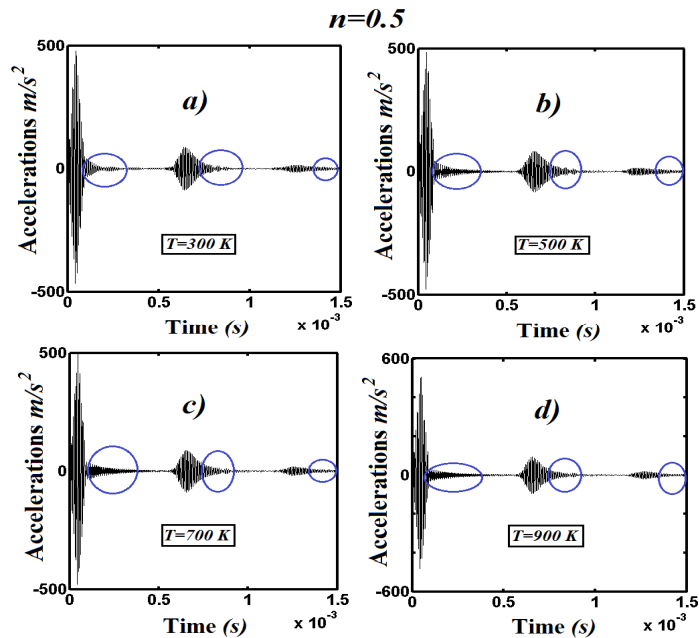


Fig. 9 Transverse accelerations at the free end of the FG beam for $n = 0.5$. (a) $T = 300\text{ K}$; (b) $T = 500\text{ K}$; (c) $T = 700\text{ K}$; and (d) $T = 900\text{ K}$

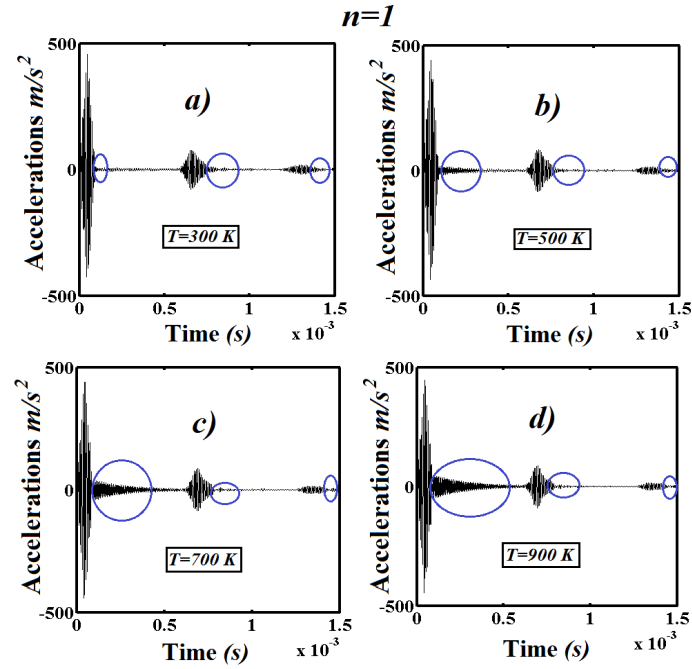


Fig. 10 Transverse accelerations at the free end of the FG beam for $n = 1$. (a) $T = 300\text{ K}$; (b) $T = 500\text{ K}$; (c) $T = 700\text{ K}$; and (d) $T = 900\text{ K}$

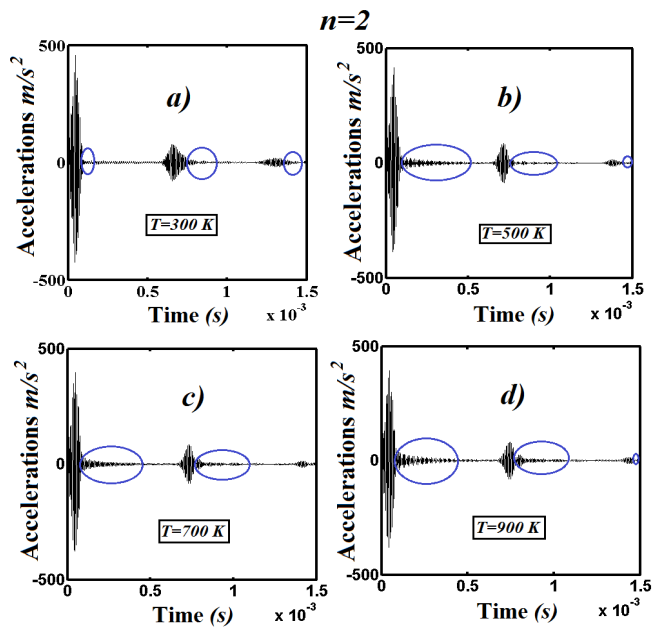


Fig. 11 Transverse accelerations at the free end of the FG beam for $n = 2$. (a) $T = 300\text{ K}$; (b) $T = 500\text{ K}$; (c) $T = 700\text{ K}$; and (d) $T = 900\text{ K}$

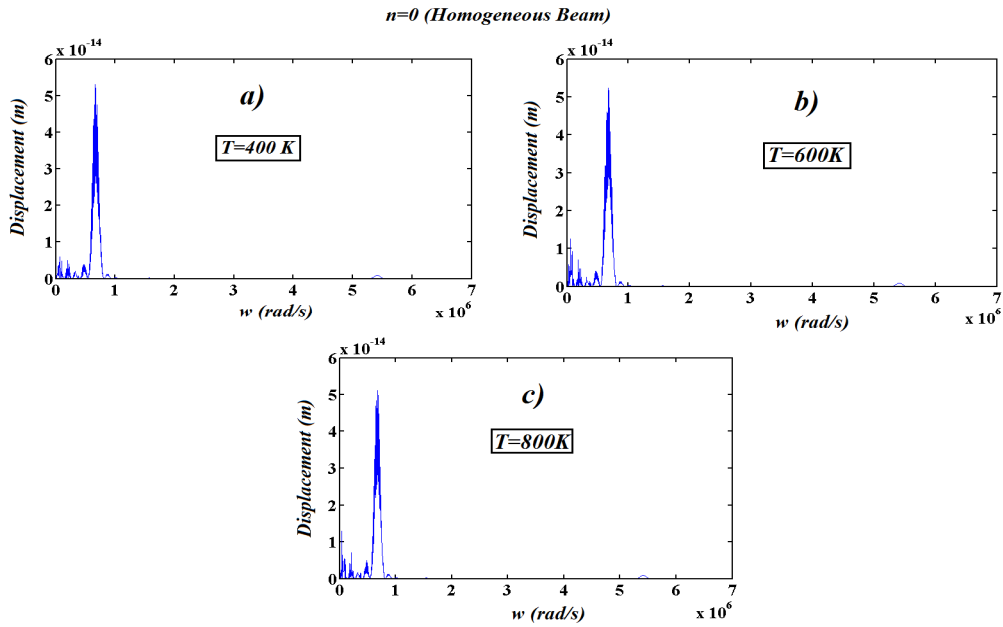


Fig. 12 Transverse accelerations at the free end of the FG beam on the frequency domain response for $n = 0$. (a) $T = 400\text{ K}$; (b) $T = 600\text{ K}$; and (c) $T = 800\text{ K}$

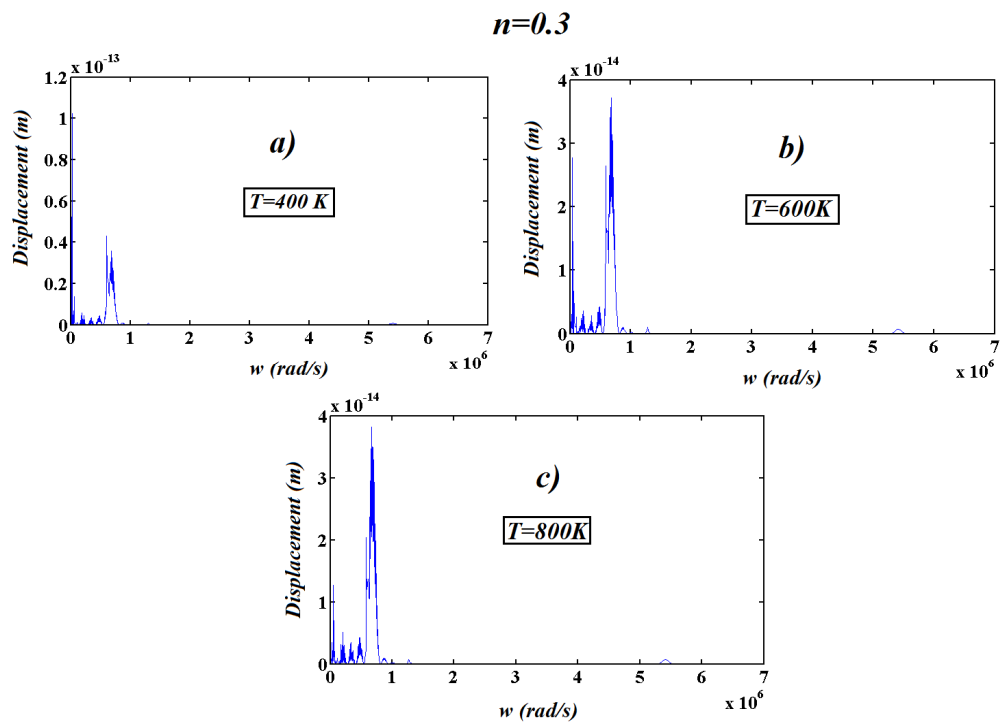


Fig. 13 Transverse accelerations at the free end of the FG beam on the frequency domain response for $n = 0.3$ (a) $T = 400\text{ K}$; (b) $T = 600\text{ K}$; and (c) $T = 800\text{ K}$

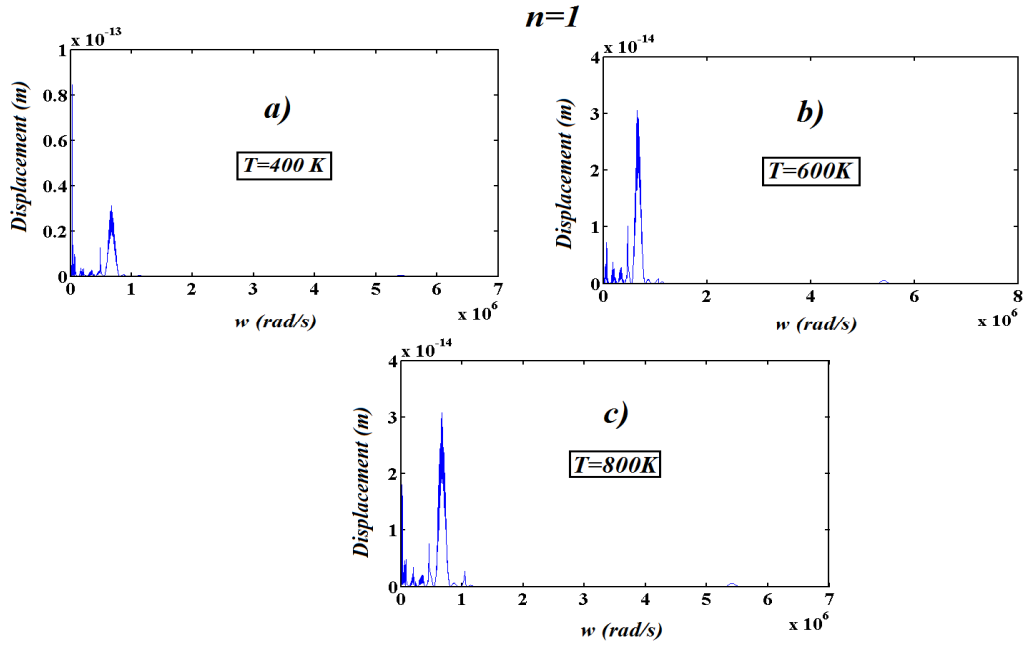


Fig. 14 Transverse accelerations at the free end of the FG beam on the frequency domain response for $n = 1$. (a) $T = 400\text{ K}$; (b) $T = 600\text{ K}$; and (c) $T = 800\text{ K}$

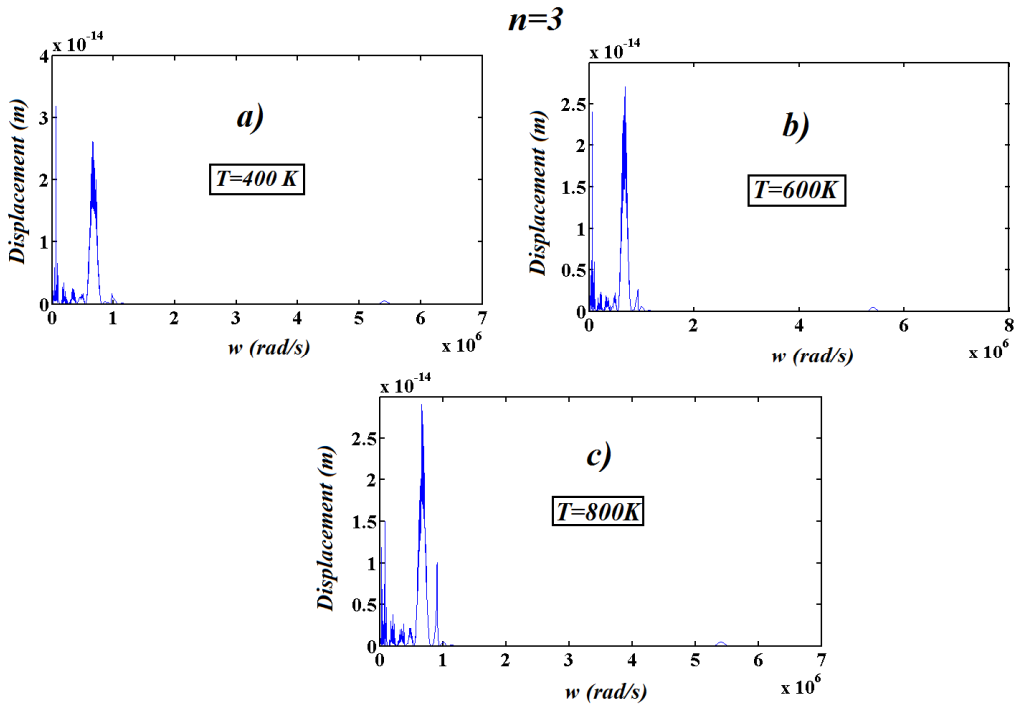


Fig. 15 Transverse accelerations at the free end of the FG beam on the frequency domain response for $n = 3$ (a) $T = 400\text{ K}$; (b) $T = 600\text{ K}$; and (c) $T = 800\text{ K}$

It is seen from Fig. 8 that three waves occur (namely the excitation and the reflected wave. The first wave, namely the excitation, is occurred by the impact force. The second and third waves (See Circle) occur because of reflecting from the boundaries of the clamped support. Also, it is seen from figures that, the waves disappear as time progressed because of the damping.

It is seen from Figs. 9, 10 and 11 that with increase the power law index n , additional waves occur at the end of the primary waves (the excitation and the reflected waves). This is because: the material properties of the beam vary continuously in the height direction and the bending rigidity and mass moment of inertia are variable over the entire height of the beam as seen from Fig. 6. However, the additional waves do not occur in the case of homogeneous beam ($n = 0$) as seen from Fig. 8, because the material distribution is uniform over the entire height of the beam. It shows that the determination of the inhomogeneous distribution or functionally graded distribution in the structures can be found by investigating the wave propagation analysis.

Also, it is seen from Figs. 9, 10 and 11 that with increase temperature, the amplitude of the additional waves increases in the case of functionally graded material. This is because: with increase in the temperature, the distribution of the material more vary over the entire height of

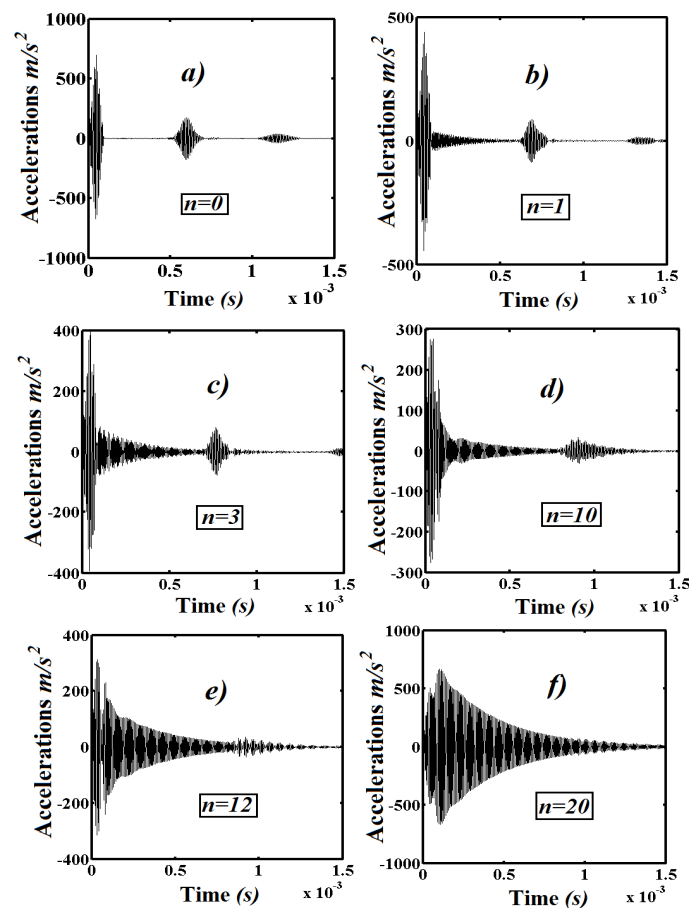


Fig. 16 Transverse accelerations at the free end of the FG beam for $T = 400$ K. (a) $n = 0$; (b) $n = 1$; (c) $n = 3$; (d) $n = 10$; $n = 12$ and $n = 20$

the beam because of temperature-dependent physically properties. Even if the temperature distribution is uniform, the bending rigidity and mass moment of inertia change over the entire height of the beam because of temperature-dependent physically properties as seen from Fig. 7. With increase temperature, due to the disorder of the material distribution increases, the effects of the inhomogeneous distribution grow. As a result, the amplitude of the additional waves increase.

It is seen from Fig. 12, with increase the temperature, the relationship between frequency (w) and displacements is almost never changed. However, it is seen from Figs. 13, 14 and 15 that with increase the temperature relationship between frequency (w) and displacements changes seriously because the disorder of the material distribution increases. It shows that the material power law index n play an important role on responses of the frequency domain of the FG beam.

In Fig. 16, the effects of the power law index n on the wave propagation of the FG beam are investigated. For this purpose, the effect of the power law index n on the transverse accelerations at the free end of the FG cantilever beam are illustrated for $T = 400$ K.

As seen from Fig. 16 that, it is mentioned before that, with increase the power law index n , the amplitude of the additional waves increases seriously. With a increase in the power law index n , the additional waves interfere more with primary waves. Whereas, the additional waves do not interfere with the primary waves in the case of homogeneous beam as seen from Fig. 16(a). It is dedicated figures that the material distributions play an important role in the wave propagation of the functionally graded beam. With using FGM, the negative effects of the waves and impact loads can be reduced.

In Figs. 17, 18 and 19, the effects of the different types of material distribution and temperatures

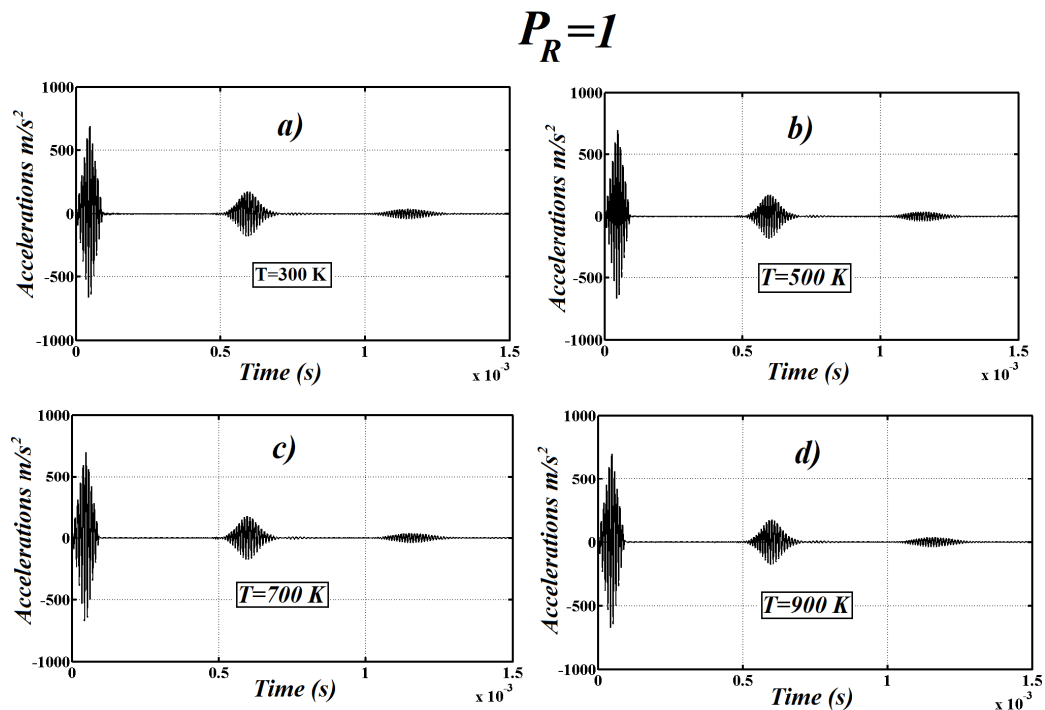


Fig. 17 Transverse accelerations at the free end of the FG beam for $P_R = 1$ for the exponential distribution. (a) $T = 300$ K; (b) $T = 500$ K; (c) $T = 700$ K; and (d) $T = 900$ K

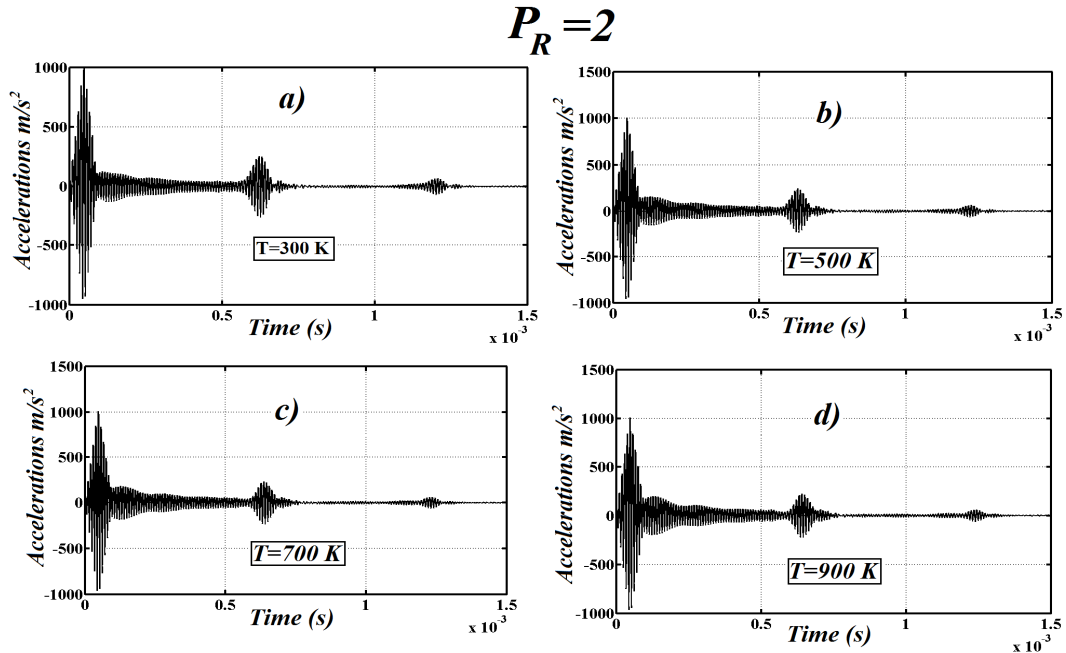


Fig. 18 Transverse accelerations at the free end of the FG beam for $P_R = 2$ for the exponential distribution. (a) $T = 300\text{ K}$; (b) $T = 500\text{ K}$; (c) $T = 700\text{ K}$; and (d) $T = 900\text{ K}$

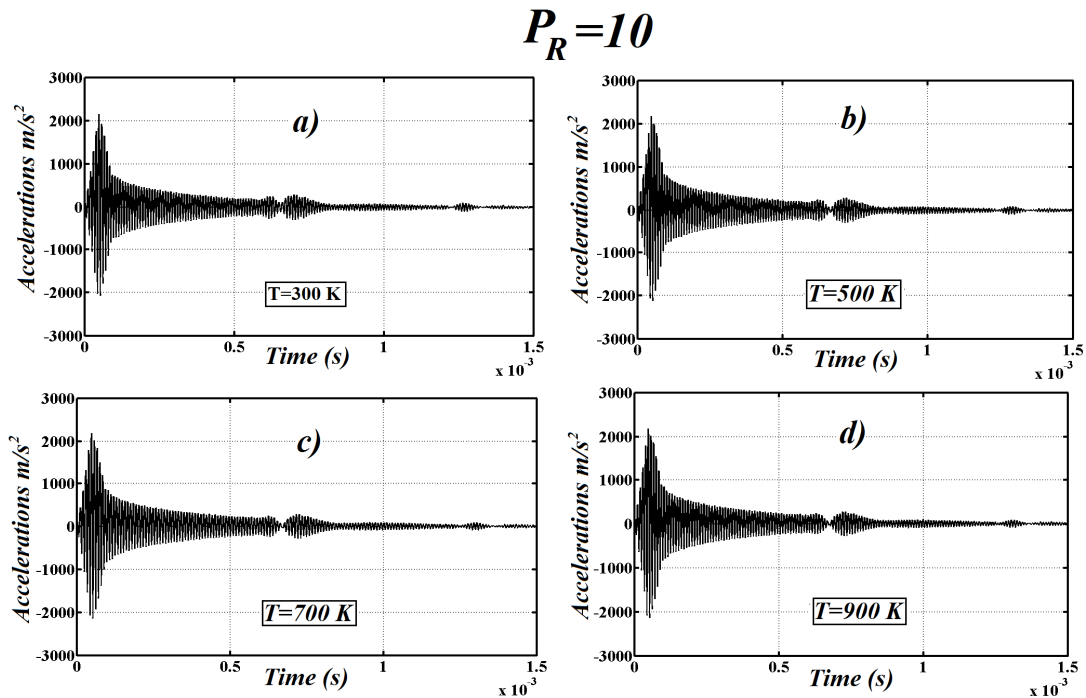


Fig. 19 Transverse accelerations at the free end of the FG beam for $P_R = 10$ for the exponential distribution. (a) $T = 300\text{ K}$; (b) $T = 500\text{ K}$; (c) $T = 700\text{ K}$; and (d) $T = 900\text{ K}$

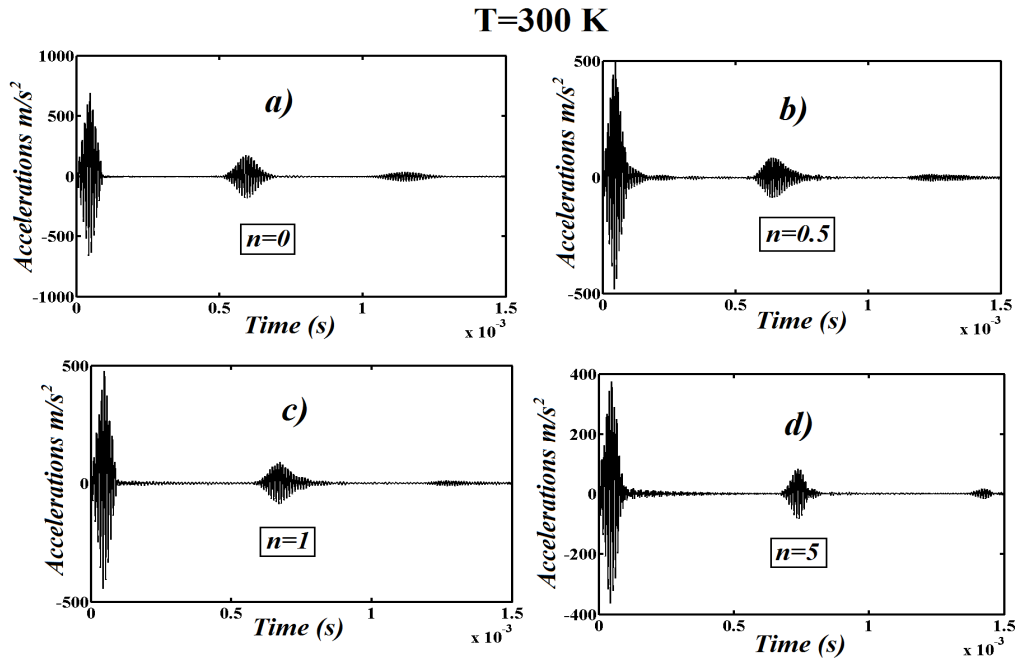


Fig. 20 Transverse accelerations at the free end of the FG beam for $T = 300$ K for the Mori–Tanaka scheme. (a) $n = 0$; (b) $n = 0.5$; (c) $n = 1$ and (d) $n = 5$

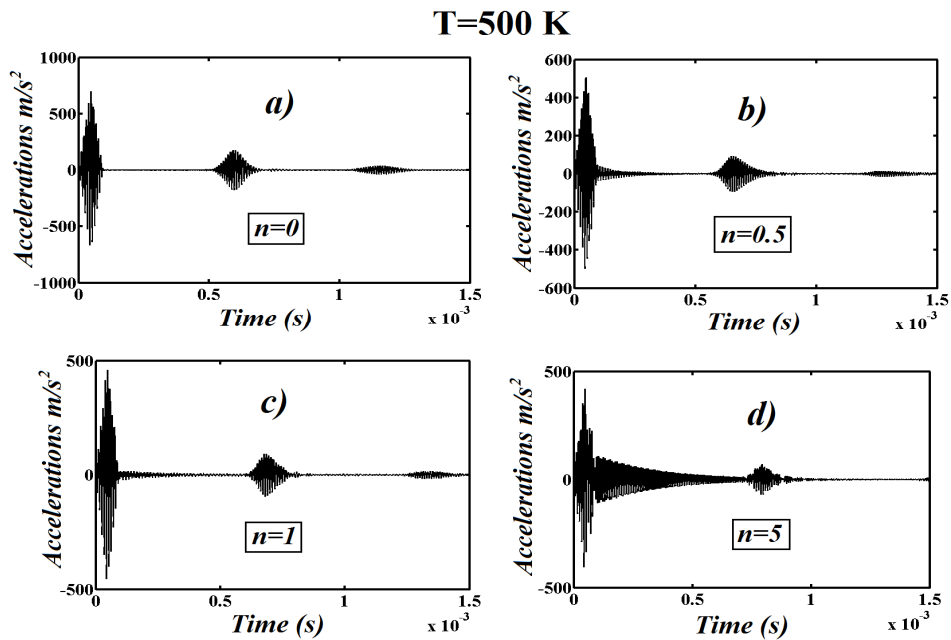


Fig. 21 Transverse accelerations at the free end of the FG beam for $T = 500$ K for the Mori–Tanaka scheme. (a) $n = 0$; (b) $n = 0.5$; (c) $n = 1$ and (d) $n = 5$

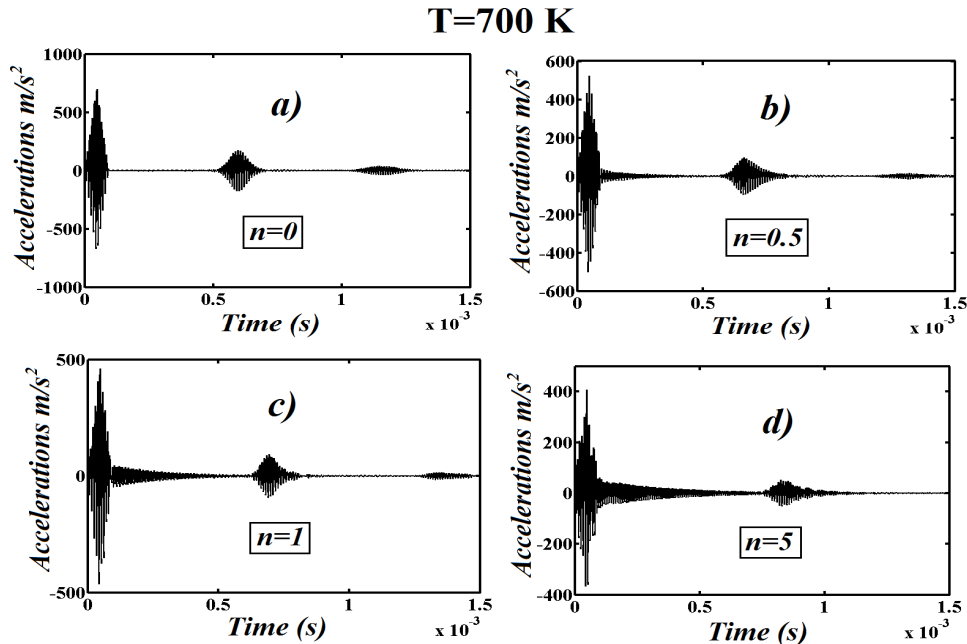


Fig. 22 Transverse accelerations at the free end of the FG beam for $T = 700$ K for the Mori–Tanaka scheme. (a) $n = 0$; (b) $n = 0.5$; (c) $n = 1$; and (d) $n = 5$

on the wave propagation of the beam are presented for the exponential distribution (Eq. (3)).

It is seen from Figs. 17, 18 and 19 that with increase the ratio of material properties $P_R (P_B / P_T)$, the amplitude of the additional waves increases seriously for the exponential distribution. Also, with increase the P_R , the additional waves interfere more with primary waves as like as the power law distribution.

In Figs. 20, 21 and 22, the effects of the different types of material distribution and temperatures on the wave propagation of the beam are presented for Mori–Tanaka scheme (Eq. (4)).

It is seen from Figs. 20, 21 and 22 that with increase the gradient index n , the amplitude of the additional waves decreases seriously for the Mori–Tanaka scheme. Also, with increase the n , the additional waves interfere more with primary waves as like as the power law and the exponential distribution. It is seen the figures, the wave propagation characteristics of the power law and the exponential distribution are almost the same. However, the wave propagation characteristics of the Mori–Tanaka scheme is different from the wave propagation characteristics of the power law and the exponential distribution.

4. Conclusions

In this paper, the effect of the temperature on the wave propagation behavior of a functionally graded cantilever beam under impact force is studied considering the temperature dependent material properties. The effects of temperature and different material distributions on the wave propagations of the FGM beams are investigated in detail. It is observed from the investigations that the temperature rising and material distributions play important role in the wave propagation

of the functionally graded beams. With increase in the temperature, the wave propagation behavior of the FG beam change seriously. Also, it is observed from the figures that the material distributions play an important role in the wave propagation of the functionally graded beam. The determination of the inhomogeneous distribution or functionally graded distribution in the structures can be found by investigating the wave propagation analysis and the additional waves. It can be reduced the negative effects of the waves by using FGM. It is necessary to consider temperature dependent material properties for getting more realistic results of the wave propagation of the FG structures under the thermal effects. Future work should be devoted to the investigation of the nonlinear wave propagation of functionally graded or different composite structures under temperature effects.

References

- Ait Yahia, S., Ait Atmane, H., Ahmed Houari, M.S. and Tounsi, A. (2015), "Wave propagation in functionally graded plates with porosities using various higher-order shear deformation plate theories", *Struct. Eng. Mech., Int. J.*, **53**(6), 1143-1165.
- Akbaş, Ş.D. (2014a), "Wave propagation analysis of edge cracked beams resting on elastic foundation", *Int. J. Eng. Appl. Sci.*, **6**(1), 40-52.
- Akbaş, Ş.D. (2014b), "Wave propagation analysis of edge cracked circular beams under impact force", *Plos One*, **9**(6), e100496.
- Akbaş, Ş.D. (2015), "Wave propagation in edge cracked functionally graded beams under impact force", *J. Vib. Control*. DOI: 10.1177/1077546314547531
- Aksoy, H.G. and Şenocak, E. (2009), "Wave propagation in functionally graded and layered materials", *Finite Elem. Anal. Des.*, **45**(12), 876-891.
- Bin, W., Jiangong, Y. and Cunfu, H. (2008), "Wave propagation in non-homogeneous magneto-electro-elastic plates", *J. Sound Vib.*, **317**(1-2), 250-264.
- Bouderba, B., Houari, M.S.A. and Tounsi, A. (2013), "Thermomechanical bending response of FGM thick plates resting on Winkler–Pasternak elastic foundations", *Steel Compos. Struct., Int. J.*, **14**(1), 85-104.
- Bourada, M., Kaci, A., Ahmed Houari, M.S. and Tounsi, A. (2015), "A new simple shear and normal deformations theory for functionally graded beams", *Steel Compos. Struct., Int. J.*, **18**(2), 409-423.
- Cao, X., Shi, J. and Jin, F. (2012), "Lamb wave propagation in the functionally graded piezoelectric-piezomagnetic material plate", *Acta Mechanica*, **223**(5), 1081-1091.
- Chakraborty, A. and Gopalakrishnan, S. (2004), "Wave propagation in inhomogeneous layered media: Solution of forward and inverse problems", *Acta Mechanica*, **169**(1-4), 153-185.
- Chakraborty, A. and Gopalakrishnan, S. (2005), "A spectral finite element for axial-flexural-shear coupled wave propagation analysis in lengthwise graded beam", *Computat. Mech.*, **36**(1), 1-12.
- Chakraborty, A., Gopalakrishnan, S. and Kausel, E. (2005), "Wave propagation analysis in inhomogeneous piezo-composite layer by the thin-layer method", *Int. J. Numer. Method. Eng.*, **64**(5), 567-598.
- Chouvion, B., Fox, C.H.J., McWilliam, S. and Popov, A.A. (2010), "In-plane free vibration analysis of combined ring-beam structural systems by wave propagation", *J. Sound Vib.*, **329**(24), 5087-5104.
- Dinevay, P.S., Rangelov, T.V. and Manolis, G.D. (2007), "Elastic wave propagation in a class of cracked, functionally graded materials by BIEM", *Computat. Mech.*, **39**(3), 293-308.
- Du, J., Jin, X., Wang, J. and Xian, K. (2007), "Love wave propagation in functionally graded piezoelectric material layer", *Ultrasonics*, **46**(1), 13-22.
- Gopalakrishnan, S. and Doyle, J.F. (1995), "Spectral super-elements for wave propagation in structures with local non-uniformities", *Comput. Method. Appl. Mech. Eng.*, **121**(1-4), 77-90.
- Farris, T.N. and Doyle, J.F. (1989), "Wave propagation in a split Timoshenko beam", *J. Sound Vib.*, **130**(1), 137-147.
- Frikha, A., Treysede, F. and Cartraud, P. (2011), "Effect of axial load on the propagation of elastic waves

- in helical beams”, *Wave Motion*, **48**(1), 83-92.
- Islam, Z.M., Jia, P. and Lim, C.W. (2014), “Torsional wave propagation and vibration of circular nanostructures based on nonlocal elasticity theory”, *Int. J. Appl. Mech.*, **6**(2), 1450011.
- Jiangong, Y. and Qiujuan, M. (2010), “Wave characteristics in magneto-electro-elastic functionally graded spherical curved plates”, *Mech. Adv. Mater. Struct.*, **17**(4), 287-301.
- Kang, B., Riedel, C.H. and Tan, C.A. (2003), “Free vibration analysis of planar curved beams by wave propagation”, *J. Sound Vib.*, **260**(1), 19-44.
- Ke, L.L., Yang, J., Kitipornchai, S. and Xiang, Y. (2009), “Flexural vibration and elastic buckling of a cracked Timoshenko beam made of functionally graded materials”, *Mech. Adv. Mater. Struct.*, **16**(6), 488-502.
- Kocaturk, T. and Akbaş, Ş.D. (2013), “Wave propagation in a microbeam based on the modified couple stress theory”, *Struct. Eng. Mech., Int. J.*, **46**(3), 417-431.
- Kocaturk, T., Eskin, A. and Akbaş, Ş.D. (2011), “Wave propagation in a piecewise homogenous cantilever beam under impact force”, *Int. J. Phys. Sci.*, **6**(16), 4013-4020.
- Krawczuk, M. (2002), “Application of Spectral beam finite element with a crack and iterative search technique to damage detection”, *Finite Elem. Anal. Des.*, **38**(6), 537-548.
- Krawczuk, M., Palacz, M. and Ostachowicz, W. (2002), “The dynamic analysis of a cracked Timoshenko beam by the spectral element method”, *J. Sound Vib.*, **264**(5), 1139-1153.
- Kumar, D.S., Mahapatra, D.R. and Gopalakrishnan, S. (2004), “A spectral finite element for wave propagation and structural diagnostic analysis of composite beam with transverse crack”, *Finite Elem. Anal. Des.*, **40**(13-14), 1729-1751.
- Lee, S.Y. and Yeen, W.F. (1990), “Free coupled longitudinal and flexural waves of a periodically supported beam”, *J. Sound Vib.*, **142**(2), 203-211.
- Li, X.Y., Wang, Z.K. and Huang, S.H. (2004), “Love waves in functionally graded piezoelectric materials”, *Int. J. Solid. Struct.*, **41**(26), 7309-7328.
- Liu, Y. and Lu, F. (2012), “Dynamic stability of a beam on an elastic foundation including stress wave effects”, *Int. J. Appl. Mech.*, **4**(2), 1250017.
- Mahi, A., Adda Bedia, E.A. and Tounsi, A. (2015), “A new hyperbolic shear deformation theory for bending and free vibration analysis of isotropic, functionally graded, sandwich and laminated composite plates”, *Appl. Math. Model.*, **39**(9), 2489-2508.
- Molaei Najafabadi, M., Ahmadian, M.T. and Taati, E. (2014), “Effect of thermal wave propagation on thermoelastic behavior of functionally graded materials in a slab symmetrically surface heated using analytical modeling”, *Compos. Part B: Engineering*, **60**, 413-422.
- Newmark, N.M. (1959), “A method of computation for structural dynamics”, *ASCE Eng. Mech. Div.*, **85**(3), 67-94.
- Ostachowicz, W., Krawczuk, M., Cartmell, M. and Gilchrist, M. (2004), “Wave propagation in delaminated beam”, *Comput. Struct.*, **82**(6), 475-483.
- Palacz, M. and Krawczuk, M. (2002), “Analysis of longitudinal wave propagation in a cracked rod by the spectral element method”, *Comput. Struct.*, **80**(24), 1809-1816.
- Palacz, M., Krawczuk, M. and Ostachowicz, W. (2005a), “The spectral finite element model for analysis of flexural-shear coupled wave propagation, Part 1: Laminated multilayer composite beam”, *Compos. Struct.*, **68**(1), 37-44.
- Palacz, M., Krawczuk, M. and Ostachowicz, W. (2005b), “The spectral finite element model for analysis of flexural-shear coupled wave propagation. Part 2: Delaminated multilayer composite beam”, *Compos. Struct.*, **68**(1), 45-51.
- Park, J. (2008), “Identification of damage in beam structures using flexural wave propagation characteristics”, *J. Sound Vib.*, **318**(4-5), 820-829.
- Reddy, J.N. and Chin, C.D. (1998), “Thermoelastic analysis of functionally graded cylinders and plates”, *J. Therm. Stress.*, **21**(6), 593-626.
- Safari-Kahnaki, A., Hosseini, S.M. and Tahani, M. (2011), “Thermal shock analysis and thermo-elastic stress waves in functionally graded thick hollow cylinders using analytical method”, *Int. J. Mech. Mater.*

- Des.*, **7**(3), 167-184.
- Shariyat, M., Khaghani, M. and Lavasani, S.M.H. (2010), "Nonlinear thermoelasticity, vibration, and stress wave propagation analyses of thick FGM cylinders with temperature-dependent material properties", *Eur. J. Mech., A/Solids*, **29**(3), 378-391.
- Shen, H.S. and Wang, Z.X. (2012), "Assessment of Voigt and Mori–Tanaka models for vibration analysis of functionally graded plates", *Compos. Struct.*, **94**(7), 2197-2208.
- Sridhar, R., Chakraborty, A. and Gopalakrishnan, S. (2007), "Wave propagation analysis in anisotropic and inhomogeneous uncracked and cracked structures using pseudospectral finite element method", *Int. J. Solid. Struct.*, **43**(16), 4997-5031.
- Sun, D. and Luo, S.-N. (2011a), "Wave propagation and transient response of a FGM plate under a point impact load based on higher-order shear deformation theory", *Compos. Struct.*, **93**(5), 1474-1484.
- Sun, D. and Luo, S.-N. (2011b), "Wave propagation and transient response of functionally graded material circular plates under a point impact load", *Compos. Part B: Engineering*, **42**(4), 657-665.
- Sun, D. and Luo, S.-N. (2011c), "The wave propagation and dynamic response of rectangular functionally graded material plates with completed clamped supports under impulse load", *Eur. J. Mech., A/Solids* **30**(3), 396-408.
- Sun, D. and Luo, S.-N. (2011d), "Wave propagation of functionally graded material plates in thermal environments", *Ultrasonics*, **51**(8), 940-995.
- Sun, D. and Luo, S.-N. (2012), "Wave propagation and transient response of a functionally graded material plate under a point impact load in thermal environments", *Appl. Math. Model.*, **36**(1), 444-462.
- Teh, K.K. and Huang, C.C. (1981), "Wave propagation in generally orthotropic beams", *Fibre Sci. Technol.*, **14**(4), 301-310.
- Tian, J., Li, Z. and Su, X. (2003), "Crack detection in beams by wavelet analysis of transient flexural waves", *J. Sound Vib.*, **261**(4), 715-727.
- Touloukian, Y.S. (1967), *Thermophysical Properties of High Temperature Solid Materials*, Macmillan, New York, NY, USA.
- Tounsi, A., Houari, M.S.A., Benyoucef, S. and Adda Bedia, E.A. (2013), "A refined trigonometric shear deformation theory for thermoelastic bending of functionally graded sandwich plates", *Aerosp. Sci. Technol.*, **24**(1), 209-220.
- Usuki, T. and Maki, A. (2003), "Behavior of beams under transverse impact according to higher-order beam theory", *Int. J. Solid. Struct.*, **40**(13-14), 3737-3785.
- Vinod, K.G., Gopalakrishnan, S. and Ganguli, R. (2007), "Free vibration and wave propagation analysis of uniform and tapered rotating beams using spectrally formulated finite element", *International Int. J. Solid. Struct.*, **44**(18-19), 5875-5893.
- Watanabe, Y. and Sugimoto, N. (2005), "Flexural wave propagation in a spatially periodic structure of articulated beams", *Wave Motion*, **42**(2), 155-167.
- Yang, J. and Chen, Y. (2008), "Free vibration and buckling analyses of functionally graded beams with edge cracks", *Compos. Struct.*, **83**(1), 48-60.
- Yokoyama, T. and Kishida, K. (1982), "Finite element analysis of flexural wave propagation in elastic beams", *Technol. Reports of the Osaka University*, **32**(1642), 103-112.
- Zhu, H., Ding, L. and Yin, T. (2013), "Wave propagation and localization in a randomly disordered periodic piezoelectric axial-bending coupled beam", *Adv. Struct. Eng.*, **16**(9), 1513-1522.
- Zidi, M., Tounsi, A., Houari, M.S.A., Adda Bedia, E.A. and Anwar Bég, O. (2014), "Bending analysis of FGM plates under hygro-thermo-mechanical loading using a four variable refined plate theory", *Aerosp. Sci. Technol.*, **34**, 24-34.

Appendix

The interpolation functions for axial degrees of freedom are

$$\boldsymbol{\varphi}^{(u)}(X) = [\varphi_1^{(u)}(X) \ \varphi_2^{(u)}(X)]^T, \quad (\text{A1})$$

where

$$\varphi_1^{(u)}(X) = \left(-\frac{X}{L_e} + 1 \right), \quad (\text{A2})$$

$$\varphi_2^{(u)}(X) = \left(\frac{X}{L_e} \right), \quad (\text{A3})$$

The interpolation functions for transverse degrees of freedom are

$$\boldsymbol{\varphi}^{(v)}(X) = [\varphi_1^{(v)}(X) \ \varphi_2^{(v)}(X) \ \varphi_3^{(v)}(X) \ \varphi_4^{(v)}(X)]^T, \quad (\text{A4})$$

where

$$\varphi_1^{(v)}(X) = \left(1 - \frac{3X^2}{L_e^2} + \frac{2X^3}{L_e^3} \right), \quad (\text{A5})$$

$$\varphi_2^{(v)}(X) = \left(-X + \frac{2X^2}{L_e} - \frac{X^3}{L_e^3} \right), \quad (\text{A6})$$

$$\varphi_3^{(v)}(X) = \left(\frac{3X^2}{L_e^2} - \frac{2X^3}{L_e^3} \right), \quad (\text{A7})$$

$$\varphi_4^{(v)}(X) = \left(\frac{X^2}{L_e} - \frac{X^3}{L_e^3} \right), \quad (\text{A8})$$

Where L_e indicates the length of the finite beam element.